Optics Letters

Mid-infrared Doppler-free saturation absorption spectroscopy of the Q branch of CH_4 $\nu_3 = 1$ band using a rapid-scanning continuous-wave optical parametric oscillator

S. M. Shah Riyadh,[1,†] Hamzeh Telfah,[2,5,†] Ian W. Jones,[2] Jonathan S. Bersson,[2] Cun-Feng Cheng,[3] Shui-Ming Hu,[3] David B. Foote,[4] and Jinjun Liu[1,2,*]

[1]Department of Physics & Astronomy, University of Louisville, Kentucky 40292, USA
[2]Department of Chemistry, University of Louisville, Kentucky 40292, USA
[3]Department of Chemical Physics, University of Science and Technology of China, Hefei, Anhui 230026, China
[4]TOPTICA Photonics Inc., 1120 Pittsford-Victor Rd., Pittsford, New York 14534, USA
[5]Current address: Department of Mechanical and Aerospace Engineering, The Ohio State University, Columbus, Ohio 43210, USA
[†]These authors contributed equally to this work.
[*]j.liu@louisville.edu

Received 17 May 2024; revised 6 July 2024; accepted 10 July 2024; posted 10 July 2024; published 22 July 2024

We have developed a mid-infrared Doppler-free saturation absorption spectroscopy apparatus that employs a commercial continuous-wave optical parametric oscillator (CW OPO), complemented by a home-built automation and wavelength scanning system. Here, we report a comprehensive spectral scan of the Q branch transitions of the $\nu_3 = 1$ band of methane (CH_4) with an average linewidth (FWHM) of 4.5 MHz. The absolute frequency calibration was achieved using previously reported transition frequencies determined using optical frequency combs, while a Fabry–Perot etalon was used for the relative frequency calibration. We report 15 transitions with improved accuracies of 1.13 MHz (3.76×10^{-5} cm^{-1}).

https://doi.org/10.1364/OL.530567

Methane (CH_4) has a long-standing interest in multiple research fields. In spite of its prominence and significance, the study of the methane molecule is complicated by a number of challenges posed by its molecular structure and properties. Methane has a high level of symmetry (T_d) that translates to a wealth of near-degenerate vibrational states that form strongly perturbed groups known as polyads. Understanding these collections of structures requires highly accurate theoretical calculations and high-resolution, high-precision spectroscopic measurements. Multiple linelists of CH_4 developed for and accessible through the databases ExoMol [1] and TheoReTS [2] have been determined via *ab initio* calculations, requiring experimental measurements to verify their accuracy and to check the theoretical spectra developed from the linelists.

One section of the mid-infrared region of particular significance, the 3.0–3.5 μm region, covers most of the pentad of CH_4 and contains nine vibrational sublevels. Of the sublevels of CH_4 that can be reached from the ground vibrational level using this range of wavelengths, the most prominent is the $\nu_3 = 1$ level (the fundamental of the antisymmetric CH stretch mode). The P, Q, and R branches of the $\nu_3 = 1$ band have been scanned individually in multiple prior experiments. (See Ref. [3] for a comprehensive review of the most recent advancements in high-resolution spectroscopy studies of CH_4.) Methane transitions in this region can be used to calibrate transition frequencies of other molecules in the mid-infrared, especially those of X–H stretch bands. The region also serves as an effective range for the pump transition in double-resonance spectroscopy measurements using an optical parametric oscillator (OPO) as the pump source, while another light source, either a diode laser [4] or an optical frequency comb [5,6], can be used as the probe to reach the triacontad and tetracontad from this range.

In the present work, the saturation absorption spectroscopy technique is used to record the Doppler-free spectrum of the Q branch of ro–vibrational (rotational–vibrational) transitions to the $\nu_3 = 1$ level of CH_4 with the idler beam of a continuous-wave (CW) OPO (Toptica, TOPO) [7] as the mid-infrared light source. The transition frequency calibrated using optical frequency combs in previously reported CH_4 spectra is used for absolute frequency calibration, while fringes in the transmission of a Fabry–Perot etalon are used for the relative frequency calibration, correcting errors in transition frequencies relative to each other, which are induced by the instability of step sizes in the wavelength scan of the OPO and the discrepancies between the measured and the real step sizes.

Our Doppler-free saturation absorption spectroscopy setup uses the conventional counter-propagating pump-probe scheme. (See Fig. 1). Briefly, the 1064 nm output of a distributed feedback (DFB) diode laser (Toptica, DFB Pro BFY) is attenuated to 3.5 mW before being seeded into a fiber amplifier (IPG, YAR-10K-1064-LP-SF) where it is amplified to ~10 W and subsequently being used as the pump beam of the OPO. The

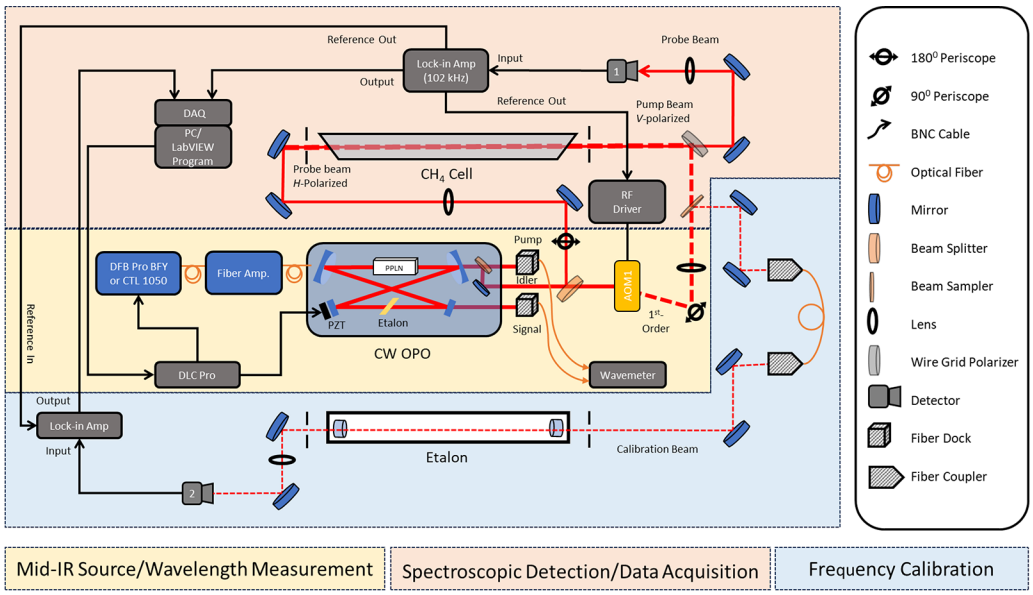

Fig. 1. Schematic diagram of the Doppler-free saturation absorption spectroscopy apparatus using a CW OPO.

wavelength of the DFB is tunable over a range of ~4 nm (35 cm^{-1}). The OPO uses a fan-out Periodically Poled Lithium Niobate (PPLN) crystal in a bow-tie ring cavity singly resonant with the signal beam. The OPO system is capable of covering the wavelength range of 1.45–4.0 µm (2500–6900 cm^{-1}) with a degeneracy gap between 2.07 and 2.19 µm. The pump and signal wavelengths (λ_P and λ_S) are measured by a wavelength meter (HighFiness WS/6-200-Vis/IR) with nominal absolute accuracy of 150 MHz (0.57 pm) and 120 MHz (0.99 pm) for λ_P and λ_S, respectively. The idler wavelength (λ_I) is determined from the former two. The linewidth of the idler was previously measured using the heterodyne technique and determined to be $\lesssim$1.8 MHz (6.0×10^{-5} cm^{-1}) with 25 ms acquisition time at a wavelength of 3.3 µm [7]. The idler output (2.19–4.0 µm) has >1 W power.

For a large change in λ_I, the position of the PPLN crystal is moved so that a different grating period of the crystal is used to achieve the quasi-phase-matching condition. Mode-selection of the signal beam is achieved by rotating an intracavity etalon. λ_I can also be continuously and rapidly tuned by temperature-tuning (up to 25 GHz/s) or current-tuning (with a repetition rate up to the MHz level between the set current points) of the DFB laser, i.e., tuning λ_P. In the present work, λ_S is fixed during a continuous wavelength scan, while the DFB wavelength is temperature-tuned to achieve large mode-hope-free (MHF) scan ranges (typically 50–100 GHz in the 3 µm region). To facilitate the wavelength change, a "look-up table" can be generated by changing the position of the PPLN crystal and the angle of the intracavity etalon and measuring the power of the idler beam at each combination. The optimal combination that maximizes the idler power at a certain frequency is recorded in the look-up table. During the spectral scan, λ_I is first changed to the requested start wavelength by changing the position of the PPLN crystal and the angle of the intracavity etalon to the optimal combination according to the look-up table, followed by the continuous wavelength scan until a mode hop occurs, indicated by a wavelength jump. Then, the OPO moves to the new start wavelength of the next continuous scan range, which partially overlaps with the previous one. MHF scans are stitched together using shared CH_4 lines or etalon fringes.

In the Doppler-free spectroscopic measurement, the idler beam is split into two by a CaF_2 beamsplitter. The reflected beam is attenuated by a variable neutral density filter to 1–2 mW and used as the probe beam of the saturation absorption measurement. The transmission of ~500 mW idler beam is modulated by an acousto-optical modulator (AOM, Brimrose, GEF-100-20-3000-WC, $f_{RF} = 100$ MHz). The square-wave modulation voltage (102 kHz repetition rate with a 50% duty cycle) is provided by the reference signal of a lock-in amplifier (SRS SR810) sent to the AOM driver (Brimrose, FF-100-B2-V7). The modulated first-order sideband has an average power of ~175 mW. Its polarization is rotated from horizontal to vertical by a 90° periscope. A sapphire wedged window is used to reflect a small portion of the first sideband (≤10 mW), which is used for relative frequency calibration. The transmission, used as the pump beam of the saturation absorption measurement, is attenuated to 50–70 mW and overlapped with the probe beam in the opposite direction using a wire-grid polarizer. The pump and probe beams are about 3 and 1.5 mm in diameter in the absorption cell, respectively. The etalon for relative frequency calibration consists of two high-reflectivity mirrors (LayerTech) mounted in an Invar frame to reduce thermal expansion and improve the stability of its free spectral range (FSR). To eliminate the FRS variation due to the small drift of the idler beam, the frequency calibration beam is coupled into and out of an optical fiber before being sent through the etalon.

The probe beam of the saturation absorption measurement and the transmission of the frequency calibration beam through the etalon are detected with liquid-N_2-cooled InSb (Infrared Associates, 449-INSB-1.0-SL8) and MCT (Kolmar Technologies, KV104-0.1-E1/KA5) photovoltaic detectors, lock-in amplified (SRS SR810 and SR530, respectively), sent to a data acquisition (DAQ) card (MCC, PCI-DAS-4020/12, 20 MHz sample rate), and recorded without averaging on the DAQ card. A step size of 0.5 MHz was used for the Doppler-free spectroscopy measurement, and a scan speed of 1 GHz/min (2000 data points/min)

was adopted, limited mainly by the time constant of the lock-in amplifier (30 ms).

The absorption cell is 85 cm long with a CH_4 pressure of $\lesssim$0.5 Torr. Given the self-pressure broadening coefficients on the level of 0.06 cm^{-1}/atm (2.4 MHz/Torr) [3], the pressure broadening makes a less significant contribution to the overall linewidth of the saturation absorption spectrum than the convoluted linewidth of the pump and probe beams ($\leq 1.8 \times \sqrt{2} \approx 2.5$ MHz) and the power broadening. The average FWHM of CH_4 transitions recorded in the present work is ~4.5 MHz, with the minimum being 2.2 MHz. Given the scan speed, it takes ~270 ms to cover a typical FWHM.

We scanned the wavelength region of ca. 3310–3325 nm (3008–3020 cm^{-1}) covering the Q branch of the $\nu_3 = 1$ band of CH_4. The Doppler-free spectrum is illustrated in Fig. 2(b) in comparison with transitions from the HITRAN database [Fig. 2(a)]. A portion of the spectrum with relatively weak, high-J transitions is illustrated in Fig. 2(c) with comb-calibrated transition frequencies labeled. Details of four transition lines in this region are shown in Fig. S.2 of Supplement 1. The line at 3010.7513 cm^{-1} demonstrates a linewidth of 2.2 MHz [also shown in the inset of Fig. 2(c)], dominated by the OPO linewidth, while the others are significantly power-broadened. The etalon fringe trace for the relative frequency calibration (finesse ~ 10) is shown in Fig. 2(d).

Transition frequencies were determined using the local-maximum method. Details of the frequency calibration and error analysis are given in Supplement 1. Briefly, the absolute frequency calibration of the CH_4 lines was done using previously reported high-accuracy transition frequencies (with uncertainty $\sigma_\nu \approx 2$ or 3 kHz) measured using optical frequency combs [8,9]. Our home-built frequency calibration program first determines the FSR of the etalon using comb-calibrated transition frequencies of selected CH_4 lines (referred to as the "reference transitions"). The lines are selected for their large transition intensities and are typically separated by 1–2 cm^{-1}. The FSR is calculated as $FSR = (f_2 - f_1)/n_{FSR}$, where f_1 and f_2 are the frequencies of two consecutive reference transitions, and n_{FSR} is their frequency separation in the unit of FSR. The fractional part of n_{FSR} is determined from the number of steps of the OPO scan. The FSR values so determined [166.38(4) MHz] are illustrated in Fig. S.3 (Supplement 1). A cubic spline interpolation is then used for frequency linearization, and the reference transitions are used to determine the absolute frequencies.

The recorded Doppler-free spectrum contains strong transitions as reported in Refs. [8,9], which are included in HITRAN with a frequency error code of 7. (In the HITRAN database, an error code of n for the line position corresponds to a frequency uncertainty between 10^{-n} and $10^{-(n-1)}$ cm^{-1}.) We chose four well-separated transitions with an frequency error code = 7 as the reference transitions for the frequency calibration, and another 12 were used to determine the accuracy of the frequency calibration procedure. (See Table S.1, Supplement 1) The 12 calibrated transition frequencies were compared to the comb-calibrated values in Refs. [8,9], yielding a mean deviation of 0.70 MHz (2.33×10^{-5} cm^{-1}) and a standard deviation of 1.13 MHz (3.76×10^{-5} cm^{-1}). Frequency calibration of the Doppler-free spectroscopic measurement of CH_4 transitions also provided an experimental determination of the accuracy of the wavelength meter in measuring the OPO idler frequency ($\nu_{\mathrm{idler}} = \nu_{\mathrm{pump}} - \nu_{\mathrm{signal}}$), which has a standard deviation of ~30 MHz or 1.1 pm at ~3.3 μm. We also recorded 15 medium- and low-intensity transitions, whose theoretically calculated frequencies were included in HITRAN with error codes = 3 or 4 [3,10–12]. Their center frequencies have been determined in our Doppler-free spectroscopy measurements with accuracies on the 1 MHz level, representing an improvement by a factor of up to 300. (See Table 1).

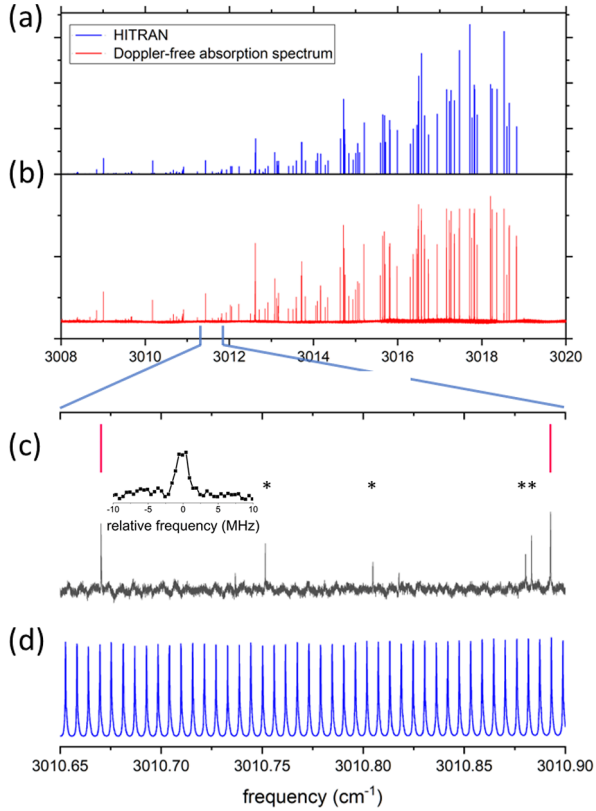

Fig. 2. (a) Q branch transitions of the $\nu_3 = 1$ band of CH_4 in the HITRAN database [3] compared to (b) Doppler-free saturation absorption spectrum obtained in the present work. (c) A portion of the Doppler-free spectrum compared to transition frequencies determined in previous frequency-comb-assisted measurements (red sticks) [8,9] used for absolute frequency calibration in the present work. Asterisked transitions are those not reported in [8,9]. Their transition frequencies were determined in the present work with accuracies on the 1 MHz level. (See text.) The inset illustrates the lineshape of the transition at 3010.7513 cm^{-1}. Panel (d) shows etalon fringes for relative frequency calibration.

In summary, we have demonstrated the viability of a rapid (2000 data points/min), high-resolution, high-frequency-accuracy spectroscopy setup with a CW OPO by recording the $\nu_3 = 1$ band of CH_4. Compared to previously reported spectra of CH_4 transitions in the same region that were recorded using a CW OPO (see, e.g. Ref. [13]), we have combined wide tunability, rapid scan speed, and a Doppler-free spectral resolution in an optical spectroscopy system. Combining the narrow linewidth with absolute and relative frequency calibration, we report transition frequencies with improved accuracy ($\sigma_\nu \approx 1.13$ MHz or 3.76×10^{-5} cm^{-1}) for 15 transitions.

The spectrum reported here was recorded in a single sweep, and a signal-to-noise ratio (S/N) of >100 was achieved for the strongest lines, thanks to the high output power of the OPO. We have detected all transitions in this wavelength region that are

Table 1. Transition Frequencies (in cm^{-1}) with Improved Accuracy in the Q Branch of the $\nu_3 = 1$ Band of CH_4 in Comparison with the Calculated Transition Frequencies Included in the HITRAN Database[a]

This Work	HITRAN	Ref.	Error Code	J''	Sym.
3009.53332	3009.533	[3]	4	15	F_2–F_1
3009.60629	3009.60540	[10]	4	15	F_2–F_1
3009.66985	3009.66956	[10]	4	14	F_1–F_2
3009.67994	3009.67940	[10]	4	14	F_2–F_1
3010.59967	3010.59924	[10]	4	15	F_2–A_1
3010.73618	3010.73645	[10]	4	15	F_2–A_1
3010.75128	3010.75162	[10]	4	14	F_2–F_1
3010.80451	3010.80413	[10]	3	14	A_1–F_2
3010.88038	3010.87992	[10]	4	15	A_1–A_2
3010.88311	3010.88304	[10]	3	13	E–E
3011.24090	3011.24028	[10]	4	14	F_1–F_2
3011.59730	3011.59718	[10]	4	14	F_2–A_1
3011.73940	3011.73862	[10]	3	14	F_2–A_1
3011.80140	3011.80115	[11]	3	14	F_1–F2
3011.82046[b]	3011.82036	[10]	4	13	F_2–F_1

[a]The transitions are labeled by the ground-state total angular momentum quantum number J'' and the symmetries of the upper-lower rotational levels.
[b]This transition is assigned to R(13) of the $\nu_2 + \nu_4$ band.

included in the HITRAN database. By data averaging, we will be able to detect more low-intensity transitions with sufficient S/N for reliable frequency calibration. A reference beam and a differential detection scheme can be used to further improve the sensitivity of the saturation absorption spectroscopy system. Also, an updated version of the CW OPO (Toptica) with higher output power (>2 W in the 3 μm region) is now commercially available, which may be used to further improve the S/N of weak transitions.

The linewidth of the OPO can be reduced by using a continuously tunable diode laser (CTL) as the seed for the fiber amplifier. Indeed, a linewidth of less than 2 MHz for the CH_4 Doppler-free spectrum has been obtained in our lab using a CTL (Toptica, CTL 1050). To further reduce the output linewidth, one can lock the OPO cavity to a seed laser [14], a molecular transition [4], or other external frequency references, e.g., an ultra-low expansion cavity and frequency combs [5,15]. To increase the scan speed, λ_I can be tuned by adjusting the voltage applied to a piezoelectric transducer (PZT) driving one mirror of the OPO cavity, i.e., tuning the signal wavelength [16].

In the present work, most medium- and low-intensity transitions are significantly power-broadened. One can attenuate the pump and probe beam powers for the saturation absorption spectroscopy measurements to reduce the spectral linewidth, although data averaging at each wavelength may be necessary to maintain the S/N.

The relative frequency calibration may be further improved by stabilizing the etalon FSR by, e.g. locking it to frequency combs [17,18] or a polarization-stabilized He–Ne laser. Alternatively, the signal and pump outputs of the OPO can be locked to an optical frequency comb and its extension, respectively, and the idler frequency can be tuned by tuning the repetition rate of the frequency comb. A linewidth on the kHz level and a sub-kHz frequency accuracy are expected using this scheme.

Funding. National Aeronautics and Space Administration-Kentucky (GF-21-053, GF-22-048); NSF Research Experiences for Undergraduates (REU) (EEC-2051002); Directorate for Mathematical and Physical Sciences (CHE-1955310).

Acknowledgment. The material includes research work supported by NASA Kentucky under NASA award No: 80NSSC20M0047. I.W.J. is supported as a NASA-Kentucky Graduate Fellow (Award No.: GF-21-053 and GF-22-048). J.S.B. was supported through an NSF Research Experiences for Undergraduates (REU) program (Grant No. EEC-2051002). This work was supported by the National Science Foundation under Grant No. CHE-1955310.

Disclosures. The authors declare no conflicts of interest.

Data availability. Data underlying the results presented in this paper are not publicly available at this time but may be obtained from the authors upon reasonable request.

Supplemental document. See Supplement 1 for supporting content.

REFERENCES

1. J. Tennyson, S. N. Yurchenko, A. F. Al-Refaie, *et al.*, J. Mol. Spectrosc. **327**, 73 (2016).
2. M. Rey, A. V. Nikitin, Y. L. Babikov, *et al.*, J. Mol. Spectrosc. **327**, 138 (2016).
3. I. E. Gordon, L. S. Rothman, R. J. Hargreaves, *et al.*, J. Quant. Spectrosc. Radiat. Transfer **277**, 107949 (2022).
4. A. Foltynowicz, L. Rutkowski, I. Silander, *et al.*, Phys. Rev. Lett. **126**, 063001 (2021).
5. Y.-D. Tan, C.-F. Cheng, Y. Tan, *et al.*, Opt. Lett. **49**, 1109 (2024).
6. V. Silva de Oliveira, I. Silander, L. Rutkowski, *et al.*, Nat. Commun. **15**, 161 (2024).
7. D. B. Foote, M. J. Cich, W. C. Hurlbut, *et al.*, Opt. Express **29**, 5295 (2021).
8. M. Abe, K. Iwakuni, S. Okubo, *et al.*, J. Opt. Soc. Am. B **30**, 1027 (2013).
9. S. Okubo, H. Nakayama, K. Iwakuni, *et al.*, Opt. Express **19**, 23878 (2011).
10. L. Daumont, A. V. Nikitin, X. Thomas, *et al.*, J. Quant. Spectrosc. Radiat. Transfer **116**, 101 (2013).
11. V. Tyuterev, S. Tashkun, M. Rey, *et al.*, J. Phys. Chem. A **117**, 13779 (2013).
12. S. Albert, S. Bauerecker, V. Boudon, *et al.*, Chem. Phys. **356**, 131 (2009).
13. P. A. Kocheril, C. R. Markus, A. M. Esposito, *et al.*, J. Quant. Spectrosc. Radiat. Transfer **215**, 9 (2018).
14. Z. T. Zhang, Y. Tan, J. Wang, *et al.*, Opt. Lett. **45**, 1013 (2020).
15. Z. T. Zhang, C. F. Cheng, Y. R. Sun, *et al.*, Opt. Express **28**, 27600 (2020).
16. A. M. Morrison, T. Liang, and G. E. Douberly, Rev. Sci. Instrum. **84**, 013102 (2013).
17. J. Wang, Y. R. Sun, L.-G. Tao, *et al.*, J. Chem. Phys. **147**, 091103 (2017).
18. G. W. Truong, D. A. Long, A. Cygan, *et al.*, J. Chem. Phys. **138**, 094201 (2013).

Supplemental Document

Optics Letters

Mid-infrared Doppler-free saturation absorption spectroscopy of the Q branch of $CH_4\nu_3 = 1$ band using a rapid-scanning continuous-wave optical parametric oscillator: supplement

S. M. Shah Riyadh,[1,†] Hamzeh Telfah,[2,5,†] Ian W. Jones,[2] Jonathan S. Bersson,[2] Cun-Feng Cheng,[3] Shui-Ming Hu,[3] David B. Foote,[4] and Jinjun Liu[1,2,*]

[1]*Department of Physics & Astronomy, University of Louisville, Kentucky 40292, USA*
[2]*Department of Chemistry, University of Louisville, Kentucky 40292, USA*
[3]*Department of Chemical Physics, University of Science and Technology of China, Hefei, Anhui 230026, China*
[4]*TOPTICA Photonics Inc., 1120 Pittsford-Victor Rd., Pittsford, New York 14534, USA*
[5]*Current address: Department of Mechanical and Aerospace Engineering, The Ohio State University, Columbus, Ohio 43210, USA*
[†]*These authors contributed equally to this work.*
[*]*j.liu@louisville.edu*

Supplement DOI: https://doi.org/10.6084/m9.figshare.26239811

Parent Article DOI: https://doi.org/10.1364/OL.530567

Supporting Information

Mid-Infrared Doppler-Free Saturation Absorption Spectroscopy of the Q Branch of CH_4 ν_3=1 Band using a Rapid-Scanning Continuous-Wave Optical Parametric Oscillator

S. M. Shah Riyadh,[1,†] Hamzeh Telfah,[2,†,‡] Ian W. Jones,[2] Jonathan S. Bersson,[2] Cun-Feng Cheng,[3] Shui-Ming-Hu,[3] David B. Foote,[4] Jinjun Liu[1,2,*]

[1]*Department of Physics & Astronomy, University of Louisville, Kentucky, 40292, USA*
[2]*Department of Chemistry, University of Louisville, Kentucky, 40292, USA*
[3]*Department of Chemical Physics, University of Science and Technology of China, Hefei, Anhui, 230026, China*
[4]*TOPTICA Photonics Inc., 1120 Pittsford-Victor Rd., Pittsford, New York, 14534, USA.*
†These authors contributed equally to this work.
‡Current address: Department of Mechanical and Aerospace Engineering, the Ohio State University, Columbus, Ohio 43210, USA.
**Corresponding author: j.liu@louisville.edu*

Received XX Month XXXX; revised XX Month, XXXX; accepted XX Month XXXX; posted XX Month XXXX (Doc. ID XXXXX); published XX Month XXXX

S.1. Frequency Calibration Procedure

In the present work, laser wavelength scanning and data acquisition were conducted simultaneously using the same LabVIEW automation and synchronization program. Frequency calibration was performed after the spectrum was recorded. The relative frequency calibration was done by cubic spline interpolation using the free spectral range (FSR) of an etalon, and the absolute frequency calibration was done using frequency-comb-calibrated transition frequencies reported in Refs. [8,9]. In this section, we describe the details of the frequency calibration procedure of the Doppler-free saturation absorption spectroscopy measurement and estimate the uncertainties of the calibrated transition frequencies.

Generally speaking, a frequency calibration procedure involves three spectra obtained simultaneously in a wavelength scan:

1. The spectrum of the molecule under study or the target molecule. Henceforward, this spectrum will be referred to as the "target spectrum", and the transitions whose frequencies need to be calibrated will be referred to as "target transitions".
2. The spectrum of the molecule used for the absolution frequency calibration, whose transition frequencies have been measured with high precision. This molecule will be referred to as the "reference molecule", its spectrum will be referred to as the "reference spectrum", and the transitions used for the absolute frequency calibration will be referred to as the "reference transitions".
3. The transmission spectrum of the etalon, whose fringes are used for the relative frequency calibration.

In the present work, the CH_4 molecule is both the target molecule and the reference molecule. The CH_4 transitions whose frequencies have been calibrated with a relative accuracy of 10^{-11} using an optical frequency comb, as reported in Refs. [8 and 9] are used as reference transitions, while the other CH_4 transitions recorded in the present work are target transitions. However, for clarity, in this section, we will still use the general case of separate target spectrum and reference spectrum to illustrate the frequency calibration procedure. Exemplary target, reference, and etalon spectra are simulated and shown in Figure S.1.

S.1.1. Determination of FSR

In the present work, the relative frequency calibration of the target spectrum is done in cubic spline interpolation using the free spectral range (FSR) of the etalon spectrum. Two reference transitions, 1 and 2, are used to determine the FSR of the etalon in the wavelength region between Reference Transitions 1 and 2. The frequency separation between the two reference transitions in the unit of the FSR is calculated as:

$$n_{\mathrm{FSR}(1,2)} = \frac{\#b - \#1}{\#b - \#a} + N_{\mathrm{FSR}}(b,c) + \frac{\#2 - \#c}{\#d - \#c} \quad \text{(S.1)}$$

where $N_{\mathrm{FSR}}(b,c)$ is the integer FSRs between the two reference transitions. (For instance, $N_{\mathrm{FSR}}(b,c) = 6$ in Figure S.1.) #1 and #2 are the positions of the two reference transitions, and #a, #b, #c, and #d are the positions of the two pairs of etalon fringes that "sandwich" the two reference transitions. Here, the "position" of a peak is measured in the step size of the scan, i.e., #n is the n^{th} data point in the spectrum. Eq. (S.1) assumes a constant frequency change for each step of the scan.

The FSR can then be calculated as:

$$\mathrm{FSR} = \frac{\Delta f_{12}}{n_{\mathrm{FSR}(1,2)}} = \frac{f_2 - f_1}{n_{\mathrm{FSR}(1,2)}} \quad \text{(S.2)}$$

where f_1 and f_2 are the high-precision frequencies of the two reference transitions.

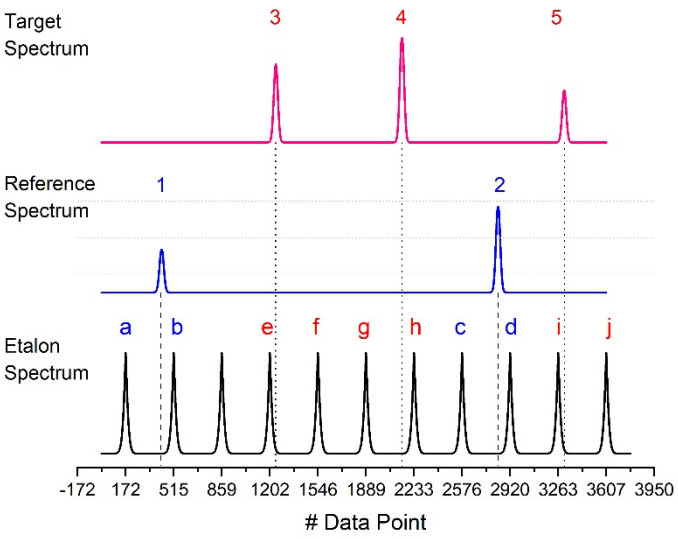

Figure S.1. Exemplary (a) target spectrum, (b) reference spectrum, and (c) etalon spectrum.

Using error propagation, we can estimate the relative accuracy of the FSR so determined:

$$\frac{\sigma_{\mathrm{FSR}}}{\mathrm{FSR}} = \sqrt{\left(\frac{\sigma_{\Delta f_{12}}}{\Delta f_{12}}\right)^2 + \left(\frac{\sigma_{n_{\mathrm{FSR}(1,2)}}}{n_{\mathrm{FSR}(1,2)}}\right)^2} \tag{S.3}$$

where σ_{FSR} is the uncertainty of the FSR value determined in Eq. (S.2). In the present work, the reference transition frequencies we used have a relative precision of 10^{-11}, and $\frac{\sigma_{\Delta f_{12}}}{\Delta f_{12}}$ is negligible. Therefore,

$$\frac{\sigma_{\mathrm{FSR}}}{\mathrm{FSR}} = \frac{\sigma_{n_{\mathrm{FSR}(1,2)}}}{n_{\mathrm{FSR}(1,2)}} \tag{S.4}$$

The relative accuracy of the FSR is equal to the relative accuracy of the frequency interval between the two reference transitions as determined in Eq. (S.1).

In Eq. (S.1), the integer number of FSRs is accurate. The combined uncertainty of the two fractional numbers of FRSs can be calculated using error propagation:

$$\sigma_{n_{\mathrm{FSR}}(1,2)} = \sqrt{\left(\frac{\#b-\#1}{\#b-\#a}\right)^2\left[\left(\frac{\sigma_{(\#b-\#1)}}{\#b-\#1}\right)^2 + \left(\frac{\sigma_{(\#b-\#a)}}{\#b-\#a}\right)^2\right] + \left(\frac{\#2-\#c}{\#d-\#c}\right)^2\left[\left(\frac{\sigma_{(\#2-\#c)}}{\#2-\#c}\right)^2 + \left(\frac{\sigma_{(\#d-\#c)}}{\#d-\#c}\right)^2\right]} \tag{S.5}$$

In the present work, spectral peaks of the target and reference transitions and the etalon fringes were determined using the local-maximum method following the necessary moving averaging of the spectrum, although fitting the lineshape could improve the accuracy in determining the peaks. We estimate that the uncertainty in determining the spectral peaks is about one step size, i.e., 0.5 MHz in the present work. The uncertainty in determining the frequency interval between two peaks is, therefore, √2x(step size). Considering the worst-case scenario that gives the largest relative uncertainty for FSR: N_{FSR}(b,c)=0 and $\frac{\#b-\#1}{\#b-\#a} = \frac{\#c-\#2}{\#d-\#c} = \frac{1}{2}$, i.e., #1 is at the middle point of #a and #b, and #2 is at the middle point of #c and #d,[1] the uncertainty in determining the number of FSRs between Reference Transitions 1 and 2 is:

$$\sigma_{n_{\mathrm{FSR}}(1,2)} = \sqrt{5}\left(\frac{\text{step size}}{FSR}\right)$$

$$n_{\mathrm{FSR}(1,2)} = 1$$

and

$$\frac{\sigma_{\mathrm{FSR}}}{\mathrm{FSR}} = \sigma_{n_{\mathrm{FSR}(1,2)}} = \sqrt{5}\left(\frac{\text{step size}}{FSR}\right)$$

For the present work, the step size is 0.5 MHz and the FSR is about 170 Hz. Therefore, for the worst-case scenario, $\frac{\sigma_{\mathrm{FSR}}}{\mathrm{FSR}}$ is about $6.5\text{x}10^{-3}$, and σ_{FSR} is about 1.1 MHz.

---

[1] If $\frac{\#b-\#1}{\#b-\#a} < \frac{1}{2}$, i.e., Reference Transition 1 is in the right half of the a-b FSR, the relative uncertainty of the FSR determined using Eq. (S.2) is smaller than the case of Transition 1 being located at the middle point of Fringes a and b. [See Eq. (S.5).]
If $\frac{\#b-\#1}{\#b-\#a} > \frac{1}{2}$, i.e., Reference Transition 1 is in the left half of the a-b FSR, we can determine the FSR based on Fringe a, instead of b, i.e.,

$$n_{\mathrm{FSR}(1,2)} = -\frac{\#1-\#a}{\#b-\#a} + N_{\mathrm{FSR}}(a,c) + \frac{\#2-\#c}{\#d-\#c}$$

The relative uncertainty of the FSR in this case is still smaller than the case of Transition 1 being located at the middle point of Fringes a and b.

In the present work, the reference transitions used to determine FSRs are usually separated by tens of FSRs. Therefore, σ_{FSR} is smaller than 0.1 MHz as shown in Figure S.2.

The selection of Reference Transitions for the determination of the FSR deserves some discussion. Under the assumption that the scan is linear, i.e., the step size is constant in frequency, and the FSR is constant between Transitions 1 and 2, a larger separation between 1 and 2 leads to a more accurate FSR as Eq. (S.4) suggests. However, smaller frequency separations between reference transitions and, hence, more reference transitions involved (if available), reduce the uncertainty in the determined FSR values due to the nonlinearity of the scan and the change of the etalon FSR due to experimental conditions, including the fluctuation of temperature and the drift of the laser beam.

S.1.2. Relative frequency calibration

The frequency of a target transition can be calculated in reference to the closest etalon fringe:

$$f_{\mathrm{target}} = f_{\mathrm{ref.}} + FSR \times n_{FSR}(\mathrm{ref.,target}) \quad \text{(S.6)}$$

where $n_{FSR}(\mathrm{ref.,target})$ is the frequency separation in the unit of FSR between the target transition and the chosen reference transition.

Using the spectra shown in Figure S.1. as an example,

$$n_{FSR}(1,3) = \frac{\#b - \#1}{\#b - \#a} + N_{FSR}(\mathrm{b,e}) + \frac{\#3 - \#e}{\#f - \#e} \quad \text{(S.7)}$$

Combineing Eqs. (S.6) and (S.7), we have:

$$f_3 = f_1 + FSR \times \left[\frac{\#b - \#1}{\#b - \#a} + N_{FSR}(\mathrm{b,e}) + \frac{\#3 - \#e}{\#f - \#e}\right] \quad \text{(S.8)}$$

Similarly, we can calibrate the frequency of Target Transition 4 based on Reference Transition 2 since Transition 4 is closer to Transition 2 than 1.

$$f_4 = f_2 - FSR \times \left[\frac{\#h - \#4}{\#h - \#g} + N_{FSR}(\mathrm{d,h}) + \frac{\#d - \#2}{\#c - \#d}\right] \quad \text{(S.9)}$$

By applying error propagation, we can estimate the accuracy of the relative frequency calibration. Again, we neglect the uncertainty of the reference frequencies. Using Target Transitions 3 as an example,

$$\frac{\sigma_{(f_3 - f_1)}}{f_3 - f_1} = \sqrt{\left(\frac{\sigma_{FSR}}{FSR}\right)^2 + \left(\frac{\#b - \#1}{\#b - \#a}\right)^2\left[\left(\frac{\sigma_{(\#b - \#1)}}{\#b - \#1}\right)^2 + \left(\frac{\sigma_{(\#b - \#a)}}{\#b - \#a}\right)^2\right] + \left(\frac{\#3 - \#e}{\#f - \#e}\right)^2\left[\left(\frac{\sigma_{(\#3 - \#e)}}{\#3 - \#e}\right)^2 + \left(\frac{\sigma_{(\#f - \#e)}}{\#f - \#e}\right)^2\right]} \quad \text{(S.10)}$$

In the present experiment, $\frac{\sigma_{FSR}}{FSR}$ is usually smaller than 10^{-3}. $\frac{\sigma_{f_3}}{f_3}$ is, therefore, almost completely dominated by the second and third terms in the square root in Eq. (S. 10). Using the same argument as above, these two terms lead to a relative uncertainty of $\frac{\sigma_{(f_3-f_1)}}{f_3-f_1}$=6.5x$10^{-3}$ for the worst-case scenario. In the present experiment, the typical separation between a target transition and its closet reference transition is on the order of 1 GHz (See Figure 2 of the main text), implying a relative frequency accuracy on the order of MHz, which is consistent with the accuracy reported in the main text. (See, also, Table S.1.)

S.1.3. Absolute frequency calibration

For each mode-hop free scan, the absolute frequency calibration is done by shifting the whole scan so that frequencies of the reference transitions match those reported in the frequency-comb-calibrated measurement.

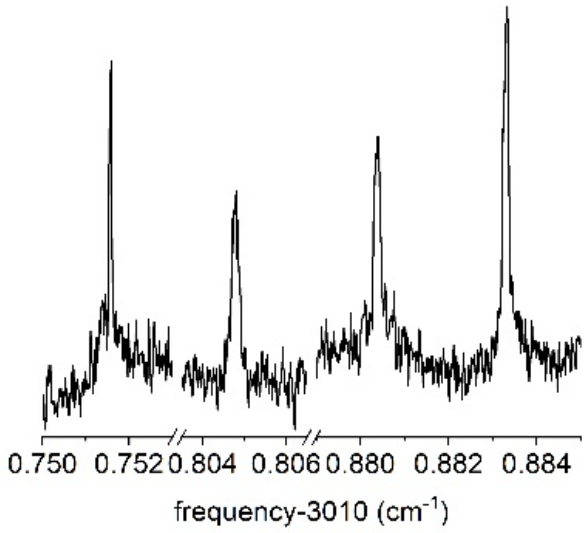

Figure S.2. Details of Doppler-free lineshapes of the asterisked transitions in Figure 2.

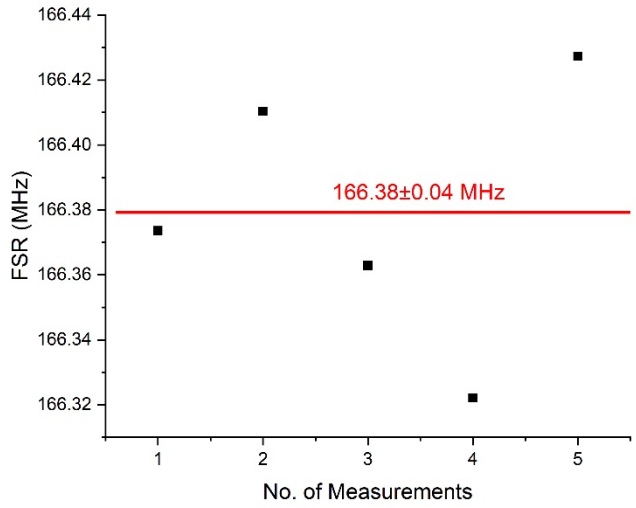

Figure S.3. Measured values of the etalon FSR.

Table S.1. Transition frequencies (in cm^{-1}) determined in the present work in comparison with the HITRAN database.

This Work	HITRAN	Error code	Deviation
3008.849035	3008.849035	7	*a*
3008.849414	3008.849399	7	-1.55E-05
3009.011367	3009.011406	7	3.94E-05
3009.533316	3009.533	4	-3.16E-04
3009.606294	3009.605398	4	-8.96E-04
3009.669854	3009.669556	4	-2.98E-04
3009.679939	3009.679401	4	-5.38E-04
3010.177852	3010.177841	7	-1.12E-05
3010.178226	3010.178258	7	3.23E-05
3010.178421	3010.178443	7	2.21E-05
3010.599665	3010.599241	4	-4.24E-04
3010.670274	3010.670274	7	*a*
3010.736177	3010.736445	4	2.68E-04
3010.751242	3010.751617	4	3.75E-04
3010.804506	3010.80413	3	-3.76E-04
3010.880354	3010.879916	4	-4.38E-04
3010.883117	3010.88304	3	-7.67E-05
3010.892709	3010.892699	7	-9.77E-06
3010.911498	3010.911498	7	*a*
3011.240853	3011.240277	4	-5.76E-04
3011.43358	3011.433641	7	6.17E-05
3011.435793	3011.435841	7	4.82E-05
3011.597299	3011.597179	4	-1.20E-04
3011.739404	3011.73862	3	-7.84E-04
3011.801433	3011.80115	3	-2.83E-04
3011.820459	3011.820363	4	-9.56E-05
3011.929742	3011.929737	7	-4.88E-06
3012.029331	3012.029331	7	*a*
3012.062686	3012.062798	7	1.11E-04
3012.229267	3012.229267	7	-4.15E-07
3012.503513	3012.503521	7	7.20E-06

[a]Used as reference transitions for frequency calibration.